Automatic Detection of Multiple and Overlapping EP Catheters in Fluoroscopic Sequences

Fausto Milletari, Nassir Navab, and Pascal Fallavollita

Chair for Computer Aided Medical Procedures, Technische Universität München, Germany
fausto.milletari@gmail.com, nassir.navab@tum.de,
fallavol@in.tum.de

Abstract. We propose a method to perform automatic detection of electrophysiology (EP) catheters in fluoroscopic sequences. Our approach does not need any initialization, is completely automatic, and can detect an arbitrary number of catheters at the same time. The method is based on the usage of blob detectors and clustering in order to detect all catheter electrodes, overlapping or not, within the X-ray images. The proposed technique is validated on 1422 fluoroscopic images yielding a tip detection rate of 99.3% and mean distance of 0.5mm from manually labeled ground truth centroids for all electrodes.

1 Introduction

Sudden cardiac death (SCD) is an unexpected death due to cardiac-related complications occurring in a short amount of time. SCD accounts for approximately 325,000 deaths per year in the United States alone. The trend of increasing SCD in developing or developed nations is thought to reflect a change in dietary and lifestyle habits in these nations. It is estimated that SCD claims more than 7,000,000 lives per year worldwide [1]. Most cases of SCD are related to cardiac arrhythmias. The most common electro physiological mechanisms leading to SCD are tachyarrhythmias such as ventricular fibrillation (VF) or ventricular tachycardia (VT). These disorders are frequently treated by radiofrequency (RF) catheter ablation. The precise localization of the arrhythmogenic site and positioning of the RF catheter at that site are problematic. These shortcomings can both reduce the efficacy of the procedure and increase the surgery time to several hours, especially with complex arrhythmias. To shorten the duration of RF catheter ablation and increase efficiency for treatment, commercial mapping systems providing 3D volume and color display of the cardiac chamber and electrical activation sequence have been developed. A review of these is presented in [2].

State-of-the-Art: In recent research practice, the medical imaging community has refocused its efforts to detect catheters directly in X-ray images. Many different types of catheters are used during EP procedures, each having specific configuration electrodes (e.g. size, shape). These electrodes are used for the measurement of electrical signals within the heart and also for the delivery of radiofrequency energy during treatment. Accurate and robust localization of catheters in the X-ray images

K. Mori et al. (Eds.): MICCAI 2013, Part III, LNCS 8151, pp. 371–379, 2013.

can provide enhanced functionality during procedures for guidance and also for post-procedural analysis. A crucial application of catheter localization is to record the position of the ablation catheter-tip in X-ray and map it onto the 3D roadmap during ablation therapies. Electrode detection methods must be robust enough to be used routinely during clinical procedures. Fallavollita *et al.* developed a catheter tip detection algorithm based on thresholds of the fluoroscopic images; this failed in low contrast images [3]. A technique for tracking and detecting the ablation catheter in X-ray images was first proposed by Franken *et al.* but the computational cost was relatively high making the method not applicable in clinic [4]. Coronary Sinus and ablation catheter detections were first proposed in [5-6]. Multiple user interaction and parameter fine-tunings were necessary to meet the quality of the X-ray image. Employing respiration and motion compensation methods may succeed in overcoming some of the above challenges [7]. Recently, Brost *et al.* developed a model-based lasso catheter tracking algorithm in biplane X-ray fluoroscopy [8-9]. However, the tracking required re- initialization and user interaction. Wen *et al.* successfully tracked one catheter in a cardiac cycle and required user-initialization in selecting tip electrodes [10-11]. The only work addressing multiple catheter tip-detection is presented in [12]. Here the authors require user interaction for their detections using a geodesic framework. In conclusion, all of the above works are excellent and demonstrate to the community how challenging the task is in achieving automatic and robust methods for electrode detection, specifically for the catheter-tip positions.

Contributions: In an effort to build upon published literature, we propose a method that considers all of the key challenges associated with catheter detections. Our automatic method: (i) detects the tip of the catheter; (ii) detects the other catheter electrodes; (iii) detects multiple catheters; and (iv) considers the overlapping scenario. We believe that the combination of these distinguish this paper making it unique in our community. Our proposed method does not rely on prior knowledge from previous X-ray frames. The aim is to obtain clinically acceptable results– an assigned error value of 2 mm for cardiac applications [13].

2 Methodology

First, our goal is to find all potential electrode candidates in X-ray. We perform these detections without the requirement of user interactivity or algorithm re-initialization. Then we aim at obtaining the highest number of candidate electrodes that correspond to real electrodes and to subsequently filter the outliers. Of the 1422 fluoroscopic images used in the evaluation, we randomly selected one X-ray frame from each dataset (a total of 20) to empirically define the algorithm parameters (Table 1).

2.1 Blob Detections

A blob detector formulation is used to detect electrodes. The electrode appearances are not always the same due to foreshortening and projective effects. They can appear

larger or smaller and their shape can change from rectangular → elliptical → circular over consecutive frames. It should be noted that for an individual X-ray image, the appearance of the electrodes belonging to the same catheter are very similar: if one of them appears as a circle it is very likely that the others share the same appearance. The candidate electrodes are obtained from a blobness measure influenced by non-maximum suppression. This blobness measure is implicitly greater than one since we are using a scale-space approach to detect electrodes at different scales. In other words, a catheter tip electrode will appear larger than the other electrodes.

Table 1. Algorithm parameter settings

Parameter	Purpose	Value	Unit	Used During
G_σ	Gaussian variance - noise reduction	1	-	preprocessing
S_σ	Start sigma for scale space creation	4	-	preprocessing
$Scales$	Number of levels (octaves) - scale space	1	-	preprocessing
$N_{samples}$	Number samples per octave - scale space	2	-	preprocessing
B_{th}	Blob detector threshold	10^{-6}	-	detection
T_{th}	Top Hat filter threshold	0.04	-	outliers rejection
S_{min}	Electrodes candidate recovery similarity value	0.85	%	electrodes recovery
$RecoveryNeigh$	Recovery neighborhood	25	px	electrodes recovery
NMS	Non maxima suppression neighborhood	3	px	electrodes recovery
P_{min}	Minimum P value for a cluster to allow blob recovery	10^{-4}	-	electrodes recovery
$ClusteringNeigh$	Clustering neighborhood	60	px	electrodes clustering
$Brightness_{min}$	Minimum brightness candidate electrodes	0.6	-	outliers rejection

We investigated two different methods that yield different performances both w.r.t. the detection rate and execution time. These approaches are based respectively on the usage of a "laplacian of gaussian" (LoG) and a "difference of gaussian" (DoG). The (LoG) blob detector [14] is a non-separable linear filter capable of finding blob-like structures while having low responses to edge-like structures. For each X-ray image it is necessary to run three linear filters and to evaluate the blobness measure:

$$Blobness_{LoG}\,(x, y, t_0) = \; t_0(L_{xx}L_{yy} - L_{xy}^2) \tag{1}$$

where L_{xx}, L_{yy}, L_{xy} are respectively the convolution of the fluoroscopic image I(x,y) with G_{xx}, G_{yy}, G_{xy} being the second derivatives of the gaussian filter and $t_0 = \sigma^2$ is used for normalization purposes equal to the variance of the gaussian filter.

The (DoG) blob detector [15] is an approximation of the "laplacian of gaussian" filter and is based only on the usage of gaussian filters that are linearly separable. A scale-space [16] representation of the image is obtained by filtering the image with a gaussian kernel using increasing variances. The difference between two neighboring scale-space images is taken and this latter result is used as a blobness measure. The mathematical formulation for the 2D gaussian filter is:

$$G(u, v, t_0) = \frac{1}{\sqrt{2\pi t_0}} e^{-(u^2+v^2)/(2t_0)} \tag{2}$$

and the blobness measure becomes:

$$Blobness_{DoG}\,(x, y, t_0) = \; I(x, y) * G(x, y, kt_0) - I(x, y) * G(x, y, t_0) \tag{3}$$

This detector has a significant response in correspondence to edge-like features in the image and thus yields more outliers (i.e. higher false positives) when compared to the LoG detector.

2.2 Rejecting Outliers via Spatial and Geometric Constraints

False positive candidate electrodes exist. To eliminate these, a Top-Hat filter is implemented which discards candidates that do not fulfill spatial and geometric constraint characteristics of an electrode. Since we are looking for "quasi circular" candidates mimicking electrodes a structuring element with a circular diameter of 15 pixels is used. This immediately removes the majority of outliers. Second, since an electrode is metallic (and thus radiopaque), it appears as a very dark cluster in the X-ray image. Thus, candidate electrodes appearing as a bright cluster are rejected. From this, the blobness measure can be used to distinguish between catheter tips and other electrodes (tip-electrodes have a stronger measure as they are larger in size).

2.3 Clustering and Catheter Detection Recovery

Clustering is then implemented to select and group those candidate electrodes that are more likely to be part of a specific catheter. We perform clustering to:

1. Reject isolated electrode detections that were not filtered out in Section 2.2.
2. Evaluate an "importance" measure $P_i = \sum_j S(b_j c_i)$ for each cluster i where b_j are the blobs of the cluster c_i. The strength measure S(.,.) is just the blobness response as it was produced by the blob detector. We will use the cluster "importance" measure in the blob recovery stage.

For a randomly selected *unvisited* blob we create a new cluster and we search the blob's neighborhood. If there are other neighbors we will add them to the current cluster and we will label the current blob as *visited.* Next, we visit the neighborhood of the candidates that we just added. Clusters containing just one blob will be deleted (they cannot be catheters).The size of the neighborhood search is specified in Table 1. **Note:** it does not matter if electrodes belonging to two or more catheters are grouped together in one cluster. As long as each one of the electrodes belonging to each catheter is inside the same cluster our method will account for this as described in the subsection 2.4.

Detection recovery is performed next. For blob clusters that have a measure P_i higher than a threshold, and for each of the candidate electrodes belonging to that cluster, we search their neighborhood to find similar structures. If the cluster i is very likely to contain a good number of true electrodes or tips (we decide this from P_i), we perform Normalized Cross Correlation in a small window around each one of the candidate electrodes to identify similar electrodes (i.e. recall that electrodes in a specific catheter share similar shape). An example of the improvement brought by the detection recovery is shown in Figure 1.

2.4 Catheter Detection and Scoring Criteria

We define a catheter as a grouping of electrodes. Prior to a cardiac ablation procedure, the electrophysiologists know the exact number of catheters that will be used. From this we formulate catheter hypotheses using the candidate electrodes detected. Then, to select the optimal global hypothesis for a specific catheter, we explore the space of possible solutions using the following greedy algorithm:

1. Knowing that *N* catheters are present in X-ray we select *N* +2 electrodes that have the strongest blobness measure. It's very likely that *N* of them will be catheter tips.
2. Starting from each of the detected tips, generate the catheter hypotheses as follows: (a) recursively create paths that include electrode candidates; (b) the created paths must be more or less straight; (c) paths should not violate any catheter geometrical constraints (length, bending angle) and be more or less straight.
3. Formulate the global hypotheses for each *N-uple* of catheters from (2) that do not share candidate electrodes.
4. Select the best global hypothesis by privileging those that contain straight and long catheters as their components.

It is not recommended to select a catheter as the ensemble of electrodes that lie on the straightest and longest path not violating the catheter geometrical constraints. This will fail since some electrodes from catheter *N+1* might be erroneously inserted in the path of catheter *N* – if the catheters are overlapping or really close to each other this effect will be predominant.

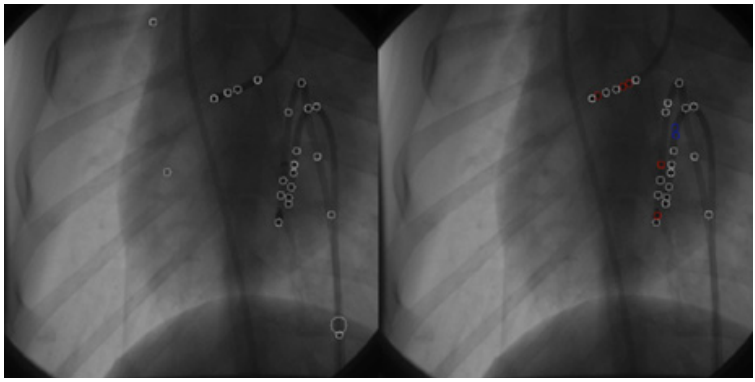

Fig. 1. (Left) blobs before clustering and recovery. (*Right*) blobs after clustering and recovery; blue - false positive detections induced by the recovery method. red – true positive detection induced by the recovery method.

Scoring Criteria via the Greedy Algorithm: for each candidate catheter the score is the number of electrodes it comprises. These electrodes cannot be in positions which are very far from the tip (< 150px selected) or that force an impossible bending angle of the catheter (< 20° selected) as stated above in solution 2. Since the maximum number of catheters in our dataset is three, we evaluate the global hypotheses in order to find the best triple of candidate catheters. The best triple is the one that comprises the longest possible candidate catheters, each one starting from one tip, that don't share any of the electrodes (e.g. the intersection of the electrodes belonging to two different candidates is always the null set). The evaluation of the best global hypotheses is done taking for each generated triple, the product of the scoring functions of the candidate catheters contained in that triple. The triple achieving the highest score is then selected. Two examples of catheter detection are presented in Figure 2.

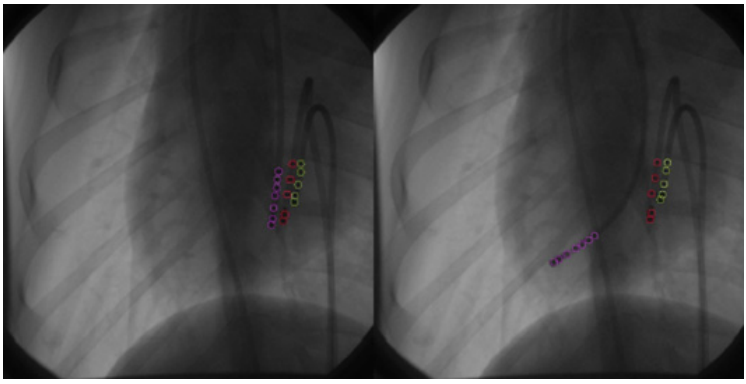

Fig. 2. Sample images depicting accurately the three catheters and their electrodes

3 Results

The method was evaluated using canine specimen laid on its right side on a fluoroscopy table (*Integris Allura, Philips Inc*.). A reference and a pacing catheter (7-French) were inserted into the right ventricle, close to the septal wall. Finally, a standard 8-French ablation catheter was inserted from the femoral vein into the left ventricle (LV) and mapped at different sites within the ventricle. A total of 20 Anterior/Posterior datasets were acquired. The image sizes are 512 × 512 with a pixel spacing of 0.44 mm. The C-arm energy was varied between 60-90kV to ensure variability within the data. In total, for one X-ray image there were 17 electrodes (3 tips + 14 other electrodes). A total of 1422 fluoroscopic frames were analyzed (i.e. 4266 tip electrodes; 19908 other electrodes; 24174 total electrodes). The centroids of the electrodes for each X-ray image were annotated manually by an expert observer. The mapping catheter is labeled as '**cat 3**', the pacing catheter as '**cat 2**' and the reference catheter as '**cat 1**'.

Detection Accuracy: Figure 3-left depicts the performances for the electrode detection using a LoG blob detector. On the horizontal axis we placed the catheters (cat1, cat2, cat3), on the vertical axis the percentage of detection of the respective electrodes (values between 0 and 1). Without the catheter recovery algorithm the detection results are: (0.68, 0.61, 0.85) and improved to (0.78, 0.78, 0.93) when performing catheter recovery. This is an 11% improvement. Similarly, Figure 3-right depicts the performances for the electrode detection using a DoG blob detector. Without the catheter recovery algorithm the detection results are: (0.81, 0.82, 0.83) and improved to (0.86, 0.88, 0.93) when performing catheter recovery. This is a 7% improvement.

Detection Precision: The mean distance of all electrodes from ground truth using a LoG blob detector with catheter recovery is 1.05 ± 0.33pixels (0.46 ± 0.14mm). Similarly, the mean distance of all electrodes from ground truth using a DoG blob detector with catheter recovery is 1.10 ± 0.52pixels (0.48 ± 0.22mm). The 95th and 99th percentile errors were 0.66mm and 0.78 mm respectively. These are well within cardiac clinical tolerances [13].

Catheter-Tips: A total of 4236 tip electrodes were automatically annotated yielding a detection rate of 99.3%. The missed detections were due to blobs being isolated away from the catheters– we observed that both the catheter tip and background of the X-ray image had similar grayscale intensity**.**

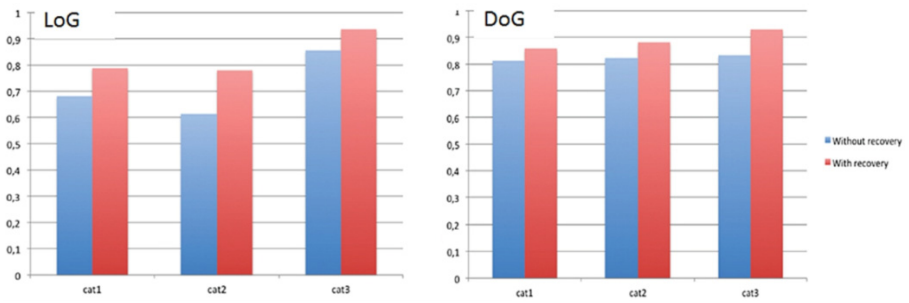

Fig. 3. Electrode detections per catheter (in %)

Outliers Per Image: Using catheter recovery, the mean number of outliers using the LoG blob detector is 10 compared to 53 for DoG. We conclude that the LoG blob detector is a more practical solution since the number of outliers is smaller; however it yields slightly less precise results compared to DoG.

Comparison to Literature: No direct numerical comparison can be made since the evaluation data, algorithm parameters, and types of catheters used differ between all published works in state-of-the art.

Processing: The algorithm was prototyped in C++ and CUDA. It has a runtime of 0.1 (LoG) and 0.3 (DoG) seconds per X-ray image using an Intel Core 2 Duo 1,86 GHz computer.

Future Work: There is room to investigate this method under various clinical conditions and different C-arm fluoroscopy devices. The variety in image quality in clinical cases is due to the variability in patient size, the variability in the image content with the presence of additional or implanted devices that were not used in our animal experiment. These will be accounted for as well as incorporating tracking in improving results [17]. Ultimately, achieving automatic detections can simplify 3D reconstruction of electrodes using single or multi-view approaches [18-19].

4 Conclusion

We introduced an automatic and robust method for multiple and overlapping catheter detection. Our method was evaluated on 1422 fluoroscopic sequences achieving 99.3% tip-detection accuracy. As expected, resolving the overlap issue and obtaining accurate electrode detections is difficult. We presented first results for these.

References

1. Mehra, R.: Global public health problem of sudden cardiac death. Journal of Electrocardiology 40(6), 118–122 (2007)
2. Fallavollita, P.: The Future of Cardiac Mapping. In: Breijo-Marquez, F.R. (ed.) Cardiac Arrhythmias - New Considerations. In Tech (2012), doi:10.5772/31068, ISBN: 978-953-51-0126-0
3. Fallavollita, P., Savard, P., Sierra, G.: Fluoroscopic navigation to guide RF catheter ablation of cardiac arrhythmias. In: Proc. 26th EMBS, vol. 1, pp. 1929–1932 (2004)
4. Franken, E., Rongen, P., van Almsick, M., ter Haar Romeny, B.: Detection of electrophysiology catheters in noisy fluoroscopy images. In: Larsen, R., Nielsen, M., Sporring, J. (eds.) MICCAI 2006. LNCS, vol. 4191, pp. 25–32. Springer, Heidelberg (2006)
5. Ma, Y., King, A.P., Gogin, N., Rinaldi, C.A., Gill, J., Razavi, R., Rhode, K.S.: Real-time respiratory motion correction for cardiac electrophysiology procedures using image-based coronary sinus catheter tracking. In: Jiang, T., Navab, N., Pluim, J.P.W., Viergever, M.A. (eds.) MICCAI 2010, Part I. LNCS, vol. 6361, pp. 391–399. Springer, Heidelberg (2010)
6. Ma, Y., Gao, G., Gijsbers, G., Rinaldi, C.A., Gill, J., Razavi, R., Rhode, K.S.: Image-based automatic ablation point tagging system with motion correction for cardiac ablation procedures. In: Taylor, R.H., Yang, G.-Z. (eds.) IPCAI 2011. LNCS, vol. 6689, pp. 145–155. Springer, Heidelberg (2011)
7. Babenko, B., Yang, M.H., Belongie, S.: Visual tracking with online multiple instance learning. In: CVPR, pp. 983–990 (2009)
8. Brost, A., Liao, R., Hornegger, J., Strobel, N.: 3-D respiratory motion compensation during EP procedures by image-based 3-D lasso catheter model generation and tracking. In: Yang, G.-Z., Hawkes, D., Rueckert, D., Noble, A., Taylor, C. (eds.) MICCAI 2009, Part I. LNCS, vol. 5761, pp. 394–401. Springer, Heidelberg (2009)

9. Brost, A., Liao, R., Hornegger, J., Strobel, N.: Respiratory motion compensation by model-based catheter tracking during EP procedures. Med. Img. Analy. 14(5), 695–706 (2010)
10. Wu, W., Chen, T., Wang, P., Zhou, S.K., Comaniciu, D., Barbu, A., Strobel, N.: Learning-based hypothesis fusion for robust catheter tracking in 2D X-ray fluoroscopy. In: CVPR, pp. 1097–1104 (2011)
11. Wu, W., Chen, T., Strobel, N., Comaniciu, D.: Fast tracking of catheters in 2D fluoroscopic images using an integrated CPU-GPU frame work. In: ISBI, pp. 1184–1187 (2012)
12. Yatziv, L., Chartouni, M., Datta, S., Sapiro, G.: Toward Multiple Catheters detection in Fluoroscopic Image Guided Interventions. T-ITB 16(4), 770–781 (2012)
13. Esteghamatian, et al.: Real-time 2D-3D MR cardiac image registration during respiration using extended Kalman filter predictors. In: 9th ICSP, pp. 1325–1328 (2008)
14. Lindeberg, T.: Detecting salient blob-like image structures and their scales with a scale-space primal sketch: a method for focus-of-attention. IJCV 11(3), 283–318 (1993)
15. Lowe, D.G., Murphy, C.: Distinctive Image Features from Scale-Invariant Key-points. IJCV 60(2), 91–110 (2004)
16. Lindeberg, T.: Scale-space. In: Encyclopedia of Computer Science and Engineering, vol. 4, pp. 2495–2540. John Wiley and Sons (2009)
17. Heibel, H., Glocker, B., Groher, M., Pfister, M., Navab, N.: Interventional tool tracking using discrete optimization. IEEE Trans. Med. Imaging 32(3), 544–555 (2013)
18. Fallavollita, P.: Is Single-View Fluoroscopy Sufficient in Guiding Cardiac Ablation Procedures? International Journal of Biomedical Imaging 2010, Article ID 631264, 13 pages (2010), doi:10.1155/2010/631264
19. Fallavollita, P.: Acquiring Multiview C-Arm Images to Assist Cardiac Ablation Procedures. European Association for Signal Processing: Journal on Image and Video Processing 2010, Article ID 871409, 10 pages (2010), doi:10.1155/2010/871409